

Evolution of hypoxia and hypoxia-inducible factor asparaginyl hydroxylase (FIH) regulation in chronic kidney disease

Anna Faivre^{1,2*}, Romain Dissard^{1*}, Willy Kuo^{3,4}, Thomas Verissimo¹, David Legouis^{1,5}, Grégoire Arnoux^{1,6}, Carolyn Heckenmeyer¹, Marylise Fernandez¹, Matthieu Tihy⁶, Renuga D. Rajaram¹, Vasiliki Delitsikou¹, Ngoc An Le⁷, Bernhard Spingler⁷, Bert Mueller⁸, Georg Schulz^{8,9}, Maja Lindenmeyer¹⁰, Clemens Cohen¹¹, Joseph M. Rutkowski¹², Solange Moll⁶, Carsten C. Scholz^{3,4,13}, Vartan Kurtcuoglu^{3,4}, and Sophie de Seigneux^{1,2,4}

¹ Department of Medicine and Cell physiology and Metabolism, University of Geneva, Geneva, Switzerland.

² Service of Nephrology, Department of Medicine, Geneva University Hospitals, Geneva, Switzerland.

³ Institute of Physiology, University of Zurich, Zurich, Switzerland

⁴ National Centre of Competence in Research, Kidney.CH, University of Zurich, Winterthurerstrasse 190, 8057 Zurich, Switzerland

⁵ Division of Intensive Care, Department of Acute Medicine, Geneva University Hospitals, 1205 Geneva, Switzerland.

⁶ Service of Clinical Pathology, Department of Pathology and Immunology, University Hospitals and University of Geneva, Geneva, Switzerland.

⁷ Department of Chemistry, University of Zurich, Winterthurerstrasse 190, 8057 Zurich, Switzerland

⁸ Biomaterials Science Center, Department of Biomedical Engineering, University of Basel, Gewerbestrasse 14, 4123 Allschwil, Switzerland

⁹ Micro- and Nanotomography Core Facility, Dept. of Biomedical Engineering, University of Basel, Gewerbestrasse 14, 4123 Allschwil, Switzerland

¹⁰ III. Department of Medicine, University Medical Center Hamburg-Eppendorf, Hamburg, Germany.

¹¹ Nephrological Center, Medical Clinic and Polyclinic IV, University of Munich, Munich, Germany.

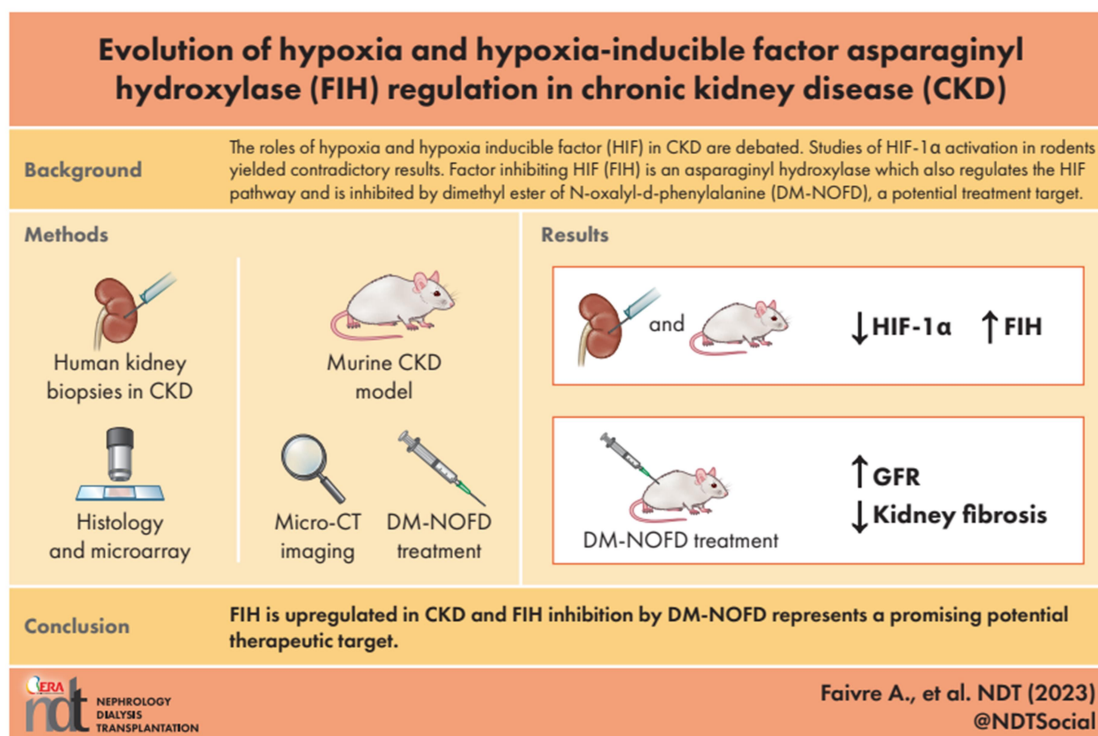
¹² Department of Medical Physiology, Texas A&M University Health Science Center, Bryan, Texas, United States of America.

¹³ Institute of Physiology, University Medicine Greifswald, Greifswald, Germany

*These authors contributed equally.

Correspondence to: Sophie de Seigneux; E-mail: Sophie.deSeigneux@hcuge.ch

GRAPHICAL ABSTRACT



ABSTRACT

Background. The roles of hypoxia and hypoxia inducible factor (HIF) during chronic kidney disease (CKD) are much debated. Interventional studies with HIF- α activation in rodents yielded contradictory results. The HIF pathway is regulated by prolyl and asparaginyl hydroxylases; while prolyl hydroxylase inhibition is a well-known method to stabilize HIF- α , little is known about the effect asparaginyl hydroxylase Factor Inhibiting HIF inhibiting (FIH).

Methods. We used a model of progressive proteinuric CKD and a model of obstructive nephropathy with unilateral fibrosis. In these models, we assessed hypoxia with pimonidazole and vascularization with three-dimensional micro-CT imaging. We analyzed a database of 217 CKD biopsies from stage 1 to 5 and we randomly collected 15 CKD biopsies from various severity degrees to assess FIH expression. Finally, we modulated FIH activity *in vitro* and *in vivo* using a pharmacologic approach, to assess its relevance in CKD.

Results. In our model of proteinuric CKD, we show that early CKD stages are not characterized by hypoxia or HIF activation. At late CKD stages, some areas of hypoxia are observed, but these are not

colocalizing with fibrosis. In mice and in humans, we observed a downregulation of the HIF pathway, together with an increased FIH expression in CKD, according to its severity. Modulating FIH *in vitro* affects cellular metabolism, as described previously. *In vivo*, pharmacologic FIH inhibition increases the glomerular filtration rate of control and CKD animals and is associated with a reduced development of fibrosis.

Conclusions. The causative role of hypoxia and HIF activation in CKD progression is questioned. A pharmacological approach of FIH downregulation seem promising in proteinuric kidney disease.

Keywords: asparaginyl hydroxylase, CKD, FIH, HIF, HIF1AN, hypoxia

ORIGINAL UNEDITED MANUSCRIPT

KEY LEARNING POINTS

What is already known about this subject?

The pathogenic role of hypoxia and hypoxia-inducible factor activation during chronic kidney disease (CKD) is currently debated.

What this study adds?

This study assesses the presence of hypoxia in a model of proteinuric kidney disease, and reveals that HIF-1 α is not upregulated in different CKD models as previously suggested; then, we show that the asparaginyl HIF hydroxylase, the Factor Inhibiting HIF (FIH), is upregulated in CKD. We further test an inhibitor of FIH, the dimethyl ester of N-oxalyl-d-phenylalanine (DM-NOFD) in conditions of CKD and show a potential protective effect.

What impact this may have on practice or policy?

This study offers new evidence to support the paradigm shift about hypoxia in CKD. Moreover, we showed that FIH inhibition in a mouse model of proteinuric CKD could improve renal function and slow down fibrosis development; this could represent a new therapeutic target in the field of CKD treatment.

ORIGINAL UNEDITED MANUSCRIPT

INTRODUCTION

Chronic kidney disease (CKD) is endemic worldwide and engenders major morbidity, mortality and health system costs (1). Currently, most of CKD cases are secondary to an initial glomerular injury leading to proteinuria (2). Focal segmental glomerulosclerosis, either primary or as secondary lesion, is a leading cause of proteinuric kidney disease (3). Proteinuria in turn is a major indicator of CKD progression (4). The pathogenesis following of CKD progression following the initial injury is much debated; in particular, the role of hypoxia and hypoxia inducible factors (HIF) transcription factors in CKD progression has been under scrutiny for several years.

Fine and colleagues emitted a few years ago the hypothesis that hypoxia was one of the major event engendering a vicious circle of CKD progression (5). This hypothesis was based on the observed loss of peritubular capillaries in CKD, leading to alterations of perfusion and oxygenation. However, since tubular cells are the major consumers of oxygen within the kidney, their atrophy and the described tubular loss of mitochondria could also decrease oxygen consumption within the kidney and balance the effects of capillary rarefaction.

The HIF pathway may play pro-inflammatory and pro-fibrotic roles participating in fibrosis (6). In this regard, genetic HIF- α downregulation seem overall protective in several models of CKD (7). However, HIF- α activation is also debated in CKD. The expression of classical HIF targets, such as VEGF, is lower rather than increased during CKD (8), which is not in agreement with an increase in HIF activity. In diabetic nephropathy, some studies even showed a decreased HIF- α activation, possibly via increased inflammation and direct inhibitory effects of glucose; in these studies, HIF- α activation prevented CKD progression (9–11). The recently developed HIF prolyl hydroxylase inhibitors (HIF-PHIs) are not only able to correct renal anemia in clinical settings (12,13), but preclinical data indicate a protective role in various murine models of CKD (14–16), even though this is questioned in the clinical setting (14). Taken together, in animal models, a continuous activation of the pathway by genetic upregulation appears detrimental. On the opposite, a transient pharmacological stimulation may be protective, which may also be related to the absence of cell specificity of the pharmacological stimulation(7).

Besides prolyl hydroxylases, which regulate HIF- α protein levels, the HIF pathway is also regulated by an asparaginyl hydroxylase called factor inhibiting HIF (FIH) (15)(16)(17). Recently, this hydroxylase was shown to be involved in several likely HIF-independent metabolic processes, such as mitochondrial biogenesis, glucose metabolism and inflammation (18,19). A global inhibition of all HIF hydroxylases, including FIH, with L-mimosine or cobalt chloride was protective in various CKD models (20,21). However, a more specific inhibition of FIH has not been tested in such models yet.

In this study, we use a murine model of progressive CKD following the apoptosis of podocytes; this model displays all the characteristics of CKD from a glomerular origin and mimics FSGS (22). In this manuscript, we assess the local presence of hypoxia, the renal micro-vascularization and HIF-1 α induction during the progression of CKD in experimental models and in kidney biopsy databases from CKD patients, as well as the expression of FIH. Then, we modulate FIH activity with a pharmacologic FIH inhibitor, the dimethyl ester of N-oxalyl-D-phenylalanine (DM-NOFD) experimentally and show a protective role of the compound on CKD progression.

MATERIALS AND METHODS

Animals

All animal studies were approved by the Institutional Ethical Committee of Animal Care in Geneva and Cantonal authorities (animal authorization numbers GE-70/19, GE-181/19 and GE14920A). Animals had free access to standard diet and water and were housed at 20°C. The proteinuric model of CKD (POD-ATTAC) was obtained as previously described (22). Briefly, POD-ATTAC male mice on FVB background were injected with dimerizer (Clontech Laboratories, Inc.) at 8 weeks. After preparation according to manufacturer datasheet, the dimerizer was injected intraperitoneally, either 0.5 μ g/g once or 0.2 μ g/g each day during 5 consecutive days. Mice were euthanized respectively after 7 days or 28 days. Littermate non-transgenic mice were used as controls and injected with the dimerizer as well. DM-NOFD (Sigma) was resuspended according to manufacturer's instructions in DMSO (ThermoFischer), diluted in 0.9% NaCl and injected at the dosage of 200mg/kg intraperitoneally during 28 consecutive days. Controls were injected with an equivalent volume of DMSO diluted in 0.9% NaCl. Unilateral urinary tract obstruction was performed as described (23,24). 8 weeks-old male mice on C57BL/6J background were used. After buprenorphine analgesia and isoflurane anesthesia, the left ureter of each mice was ligated; the right kidneys, non-obstructed, were used as controls. Organ collection occurred 7 days after the surgery.

Renal function assessment

Glomerular filtration rate was measured transcutaneously by measuring the excretion rate of fluorescein isothiocyanate sinistrin (Fresenius Kabi) with a minicamera (Medibeacon) as described previously (24). Filtration was calculated with the appropriate formula (25) in milliliter per minute per kilogram of body weight, then normalized to controls and expressed as fold change.

Kidney perfusion

POD-ATTAC mice received a terminal injection of pentobarbital injection (Inresa). The superior mesenteric artery, coeliac artery, abdominal artery and inferior vena cava were isolated and ligated, then the vena cava and the aorta were catheterized. A Prismaol 4-based solution enriched with hematocrit 10% and appropriate electrolytes was used. This solution was oxygenated with a mix of O₂ and CO₂ (95%/5%), at a flow rate of 2 L/min, through a membrane oxygenator (Medos Hilite). The oxygen partial pressure was maintained around 30 kPa in the perfusion solution. VO₂ measurement was performed after 20mn of kidney flushing and 40mn of perfusion at 350 µL/min, using an ABL90 Flex analyser (Radiometer).

Cell culture

mpkCCD (RRID:CVCL_R771), mCCD_{cl1} (26) and immortalized human proximal tubular HK-2 cells (ATCC CRL-2190) were used and cultured as described previously (27,28). Cells were transfected with plasmids expressing human wildtype FIH-V5 or siRNA targeting human FIH as described before (29,30), during 24 hours. Empty vectors or control siRNAs were transfected in parallel. The sequences for siRNAs are provided in **Resources Table**. The oxygen consumption rate of the cells was measured using Sea Horse Analyser XF96 (Agilent Technologies), using the Seahorse XFp Cell Mito Stress Test Kit (103010-100) according to manufacturer's instructions.

Erythropoietin measurement

The erythropoietin levels in the plasma were measured using the Quantikine® ELISA (MEP00B) according to manufacturer's instructions. Briefly, the blood was collected by intracardiac sampling and centrifuged at 2000g during 10 minutes. The supernatant was collected and diluted to half before the ELISA.

Histology and immunohistochemistry

Kidneys were fixed in 4% paraformaldehyde (Alfa Aesar), paraffin embedded and a 5 µm section was cut with a microtome. To perform fibrosis quantification, we proceeded as described previously (24). Briefly, a median section of the kidney was selected and stained with Sirius Red solution (Abcam), according to the manufacturer's protocol. The slides were scanned with Axioscan image scanner (Zeiss) at 20x magnification. The cortical area was manually defined and red-stained areas were automatically quantified by Definiens Tissue Phenomics® software. Immunostainings were performed

using citrate buffer (10 mM, pH 6) microwave-based antigen target retrieval technique and the EnvisionFlex kit from Dako. The antibodies used are listed in the **Resources Table**. Detection of local tissue hypoxia was performed using Hypoxyprobe™-1 Kit (Hypoxyprobe/HP1-1000) (HP1-1000Kit). 60 minutes before euthanasia, mice received an intraperitoneal injection of Hypoxyprobe™-1 at a dosage of 60mg/kg in saline. The immunostaining of pimonidazole adducts in formalin-fixed, paraffin-embedded tissue was performed according to the method described below.

Western blotting

Kidney tissue samples were homogenized in 100 µl or 1 ml respectively in cold lysis buffer (20 mmol/L Tris-HCl; 2 mmol/L EDTA; 30 mmol/L NaF; 30 mmol/L NaPPi; 0.5 mol/L Na₃VO₄; 20% SDS; 10% Triton-X-100 and Roche-Complete mini protease inhibitor mixture) on ice. Proteins were prepared in solution containing Tris-HCL 50mM, Glycerol 10%, Sodium dodecyl sulfate 1%, Bromophenol blue 0.01% and 2-Mercaptoethanol 10mM, then heated for 5 minutes at 95°C. Protein concentration assay was performed using both BCA protein Assay (Thermo Scientific, PIERCE) and Coomassie Blue gel staining (Thermo Scientific GelCode blue stain Reagent). 25µg of proteins were loaded in 10% bis-acrylamide homemade gels, and migration was performed at 100V during 1 hour. Transfer was made on nitrocellulose membrane (GE Healthcare, Life sciences) during 1 hour at 100V. After washes in TBS-Tween 0,1% (Tris-HCL 50mM, Sodium chloride 150mM and Tween20 0,1%) and blocking at room temperature in 5% milk-TBS-Tween during 1 hour, the membrane was incubated overnight at 4°C with primary antibody diluted in 5% milk-TBS-T. After washings, membrane was then incubated 1h with goat anti-rabbit HRP secondary antibody (1:5000) or goat anti-mouse HRP secondary antibody (1:10 000). All antibody references are provided in the **Resources Table**. Protein expression was detected with ECL detection reagent WesternBright Quantum (Advansta), whose chemiluminescence was revealed with PXi gel imaging system (Syngene). Band density was quantified using ImageJ software (NIH). Protein expression was normalized to Ponceau staining. Results are expressed as fold change in protein expression compared to the control samples.

Human kidney biopsies immunohistochemistry and immunofluorescence

Human kidney biopsies were collected within the Service of Pathology from Geneva University Hospitals. Tissues were fixed in formaldehyde, embedded in paraffin and cut in 3 µm thick sections. 14 samples were randomly selected and included in this study, with various renal disease and degrees of renal fibrosis and renal function. Renal fibrosis was graded after standard analyses by an experimented renal pathologist. Sections were incubated with a polyclonal rabbit anti-FIH antibody (1:100), as described previously (31). Slides were digitized, and graded in terms of FIH expression by two nephrologists in a blinded fashion. Each patient provided informed consent before inclusion in the study. The institutional ethical committee board approved the clinical protocol (CEREH number 03-081). The research was performed according to the Helsinki's declaration principles.

For immunofluorescence, 12 biopsies from 12 CKD patients and 3 non injured human kidneys (autopsy cases) were sliced at 4µm and incubated all together (one batch experiment) overnight at 4°C with HIF-AN polyclonal antibody (ab187524, 1/50 dilution) followed by 1 hour incubation at room

temperature with secondary IgG CY3 conjugated antibody (AB2338000, 1/200 dilution). Nucleus were stained with DAPI for 10 minutes at room temperature (1/1000) and mounted with Vectashield (Vector Laboratories Inc., Newark, USA). After staining, all slices were scanned with the same setting on a widefield scanner Axioscan Z1, Zeiss, Oberkochen, Germany) at 20x magnification. The renal cortex was annotated in QuPath (V0.4.2) excluding glomeruli and a detection of nuclei was performed using StarDist. Then, a random tree (RTrees) was trained to classify interstitial, tubular negative, and tubular positive cells in the 12 biopsies and 3 control kidneys. The number of positive tubular cells was expressed as a ratio of total tubular cells.

Microarray data analyses of human kidney biopsies

Published Affymetrix microarray expression data from the European Renal cDNA Kröner-Fresenius Biopsy Bank (CKD: GSE 99340, LDs: GSE32591, GSE35489, GSE37463) were analysed for mRNA expression levels of HIF hydroxylases. Sample collection, RNA isolation and preparation, and microarray analysis were performed as described previously (32). Biopsies from different kidney diseases were used (cadaveric donor (CD), tumor nephrectomy (TN), diabetic nephropathy (DN), thin basement disease (TMD), minimal change disease (MCD), hypertensive nephropathy (HTN), IgA nephropathy (IgA), focal segmental glomerulosclerosis (FSGS), membranous nephropathy (MGN), lupus nephritis (LN) and ANCA-vasculitis (ANCA) and grouped into different CKD stages (CKD1-5) according to their estimated GFR calculated by the CKD-EPI equation (33). Pre-transplantation kidney biopsies from healthy living donors served as the control group. To identify differentially expressed genes the SAM (Significance analysis of Microarrays) method was applied using TiGR (MeV, Version 4.9) (34). A q-value below 5% was considered to be statistically significant.

Real-time quantitative PCR

Total RNA from cells and kidney tissue samples was extracted with Trizol reagent (Invitrogen) or with the RNA extraction kit (Machery-Nagel) according to the manufacturer's instructions. RNA concentration and purity were measured using the NANODROP 2000C Spectrophotometer (Thermo scientific). 1µg of total RNA was reverse transcribed using qScript cDNA supermix (Quanta Biosciences). cDNA was used to perform quantitative PCR in triplicate using PowerUp SYBR Green master Mix (Applied biosystems) and StepOne Plus Real-Time PCR System (AB Applied Biosystems) or a QuantStudio 5 Real-Time PCR System (Thermo Fisher Scientific). The $2^{-\delta\delta CT}$ method was used to analyse the relative changes in gene expression levels. Primers used in quantitative PCR are listed in the **Resources Table**.

Micro-CT imaging and analysis

Mice were perfused with the in-house developed X-ray contrast agent XlinCA. Sample preparation and analysis was performed as described previously in (35). XlinCA was synthesized as described previously (36)(37)(38). After anaesthesia with ketamine/xylazine, kidneys were perfusion-fixed via the abdominal aorta and then injected with XlinCA contrast agent. The abdominal aorta was cannulated with a blunted 21 G butterfly needle, then the abdominal aorta and mesenteric artery were ligated. A

window was cut into the vena cava as an outlet, then the kidneys were flushed with first 10 ml of phosphate-buffered saline (PBS) to remove blood, then fixed with 100 ml 4% formaldehyde / 1% glutaraldehyde in PBS at 37 °C with 150 mmHg pressure. To avoid premature crosslinking, 20 ml PBS and then 50 ml glycine solution (5 mg / ml in PBS) were used to remove and quench residual aldehydes. Kidneys were then flushed again with 40 ml PBS. 3 ml of XlinCA contrast agent dissolved in water (75 mg iodine/ml) were injected with a pressure-actuated syringe, then 4% glutaraldehyde in PBS were dripped into the abdominal cavity for crosslinking. After gelation, kidneys were removed and immersed in 15 ml 4% glutaraldehyde / PBS. Before scanning, kidneys were mounted embedded in 1% agar in PBS in standard 1.5 ml centrifugation tubes. Kidneys were scanned at 4.444 μm voxel size using a General Electric Phoenix Nanotom m X-ray μCT , with a tungsten target, 90 kV acceleration voltage and 200 μA beam current. For each of the 1440 projections, nine frames with 0.5 s exposure time were recorded and averaged, resulting in a scan time of approximately 6 h for the three height steps required per kidney. 3D volumes were reconstructed using the manufacturer's proprietary GE phoenix datos|x software. Image processing was performed in a blinded fashion on a workstation equipped with 256 GB RAM and 32-core AMD 3970X threadripper processor and a Samsung 860 EVO S-ATA SSD. Datasets were 3D Gauss-filtered ($\sigma = 1$ pixel), manually thresholded to extract the blood vessels and exported as a stack of 2D TIFF images using Fiji/ImageJ software (39) (40). They were then further processed using the commercial XamFlow software (LucidConcepts AG, Zurich). The largest connected component was extracted from the thresholded binary masks to remove particles of contrast agent on the outside of the kidneys. The signed distance transform of the resulting blood vessel segment was then calculated. A mask of the kidney outer shape was created using morphological closing with 50 pixels (corresponding to 222.2 μm) and applied to the signed distance transform. All these morphological operations were performed using the CLIP library, which is capable of leveraging the full parallel processing power of the workstation. For quantification, the cumulative distribution function of the calculated distance values were calculated and evaluated at 20 μm and 100 μm using an unpaired, two-tailed Student's t-test implemented in R.

Single cell RNA-sequencing data analysis

scRNAseq data were downloaded from the following repository: <https://doi.org/10.5281/zenodo.4059315>. Data were further preprocessed using the standard Seurat workflow. Briefly, we performed, for each sample, normalization and variance stabilization with the `sctransform v2` function of Seurat. We thus applied the `RunPCA`, `RunUMAP`, `FindNeighbors` and `FindClusters` functions with default parameters. To compare gene expressions among conditions, we used the `PrepSCTFindMarkers` and the `FindMarkers` functions. Finally, we used PROGENY to infer pathways activity from gene expression

Statistics

Group's statistics were analyzed by t test and two-way ANOVA/Bonferroni's Multiple Comparison Test respectively for two or three groups. Results are expressed as fold change to controls unless specified otherwise.

RESULTS

Early stages of proteinuric CKD are not characterized by hypoxia or HIF activation

Single dose dimerizer injection led to proteinuria, modest GFR decline and inflammation, as previously described (28), without marked fibrosis (**Figure 1A**). Hypoxia was not detected by pimonidazole staining in the early CKD progression stages (**Figure 1A**). Protein expression of HIF-1 α was decreased, as well as one of its targets GLUT1 (**Figure 1B**). In RNA sequencing analysis, the global state of activation of the hypoxia pathway was assessed using the the hypoxia PROGENy pathway (41), which was also globally downregulated, together with an increase in the classically activated pro-fibrotic and pro-inflammatory pathways (**Figure 1C**), suggesting that HIF activation is not an early event in CKD. qPCR analysis confirms a decreased expression of HIF- α target genes despite a downregulation of PHDs expression (**Figure 1D**).

In late stages of proteinuric CKD, vascularization is rarefied but does not induce general tissue hypoxia

After the injection of repeated small doses of dimerizer, mice developed classical features of CKD within 28 days, with decreased measured GFR and albuminuria (24). We further observed extensive fibrosis and tubular atrophy (**Figure 2A**). Pimonidazole staining indicate the presence of hypoxia in some minor zones in already advanced CKD, but these areas were overall rare and did not colocalize with fibrotic areas (**Figure 2A and Supplementary Figure 1**). These areas were located in zones of preserved tubular morphology, in which the intact proximal tubular cells likely consume more oxygen than the atrophic cells in fibrotic tissue. Intratubular protein casts present a nonspecific staining, which should not be considered. We also observed a downregulation of HIF-1 α protein and its target GLUT1, which was even more severe than at early stages (**Figure 2B and Supplementary Figure 2A**). Like in early stages, the hypoxia Progeny pathway was downregulated and pro-inflammatory or pro-fibrotic pathways were increased (**Figure 2C**). We confirmed by qPCR the downregulation of the pathway (**Supplementary Figure 2B**). In this model, we previously confirmed that tubular cell number was not decreased (31), precluding decreased tubular mass as an explanation for these observations. We assessed renal vascularization by micro-CT after contrast agent perfusion, as described previously (42). We observed a decrease of vascular bundles mainly in the inner stripe of the outer medulla, but less in the cortex, of POD-ATTAC mice (**Figure 2D**). A certain amount of capillary rarefaction was

present (**Figure 2D, 2E and Supplementary Figure 2C**); however, 98% of the analyzed kidney tissue was close enough (100 μ m) from a vessel to be within the oxygen diffusion limit (**Figure 2E**). In a model of *ex vivo* isolated-perfused kidney (31), oxygen consumption decreased with CKD (**Figure 2F**). Therefore, given the decreased consumption and a capillary rarefaction that did not reach the oxygen diffusion limit, most areas of the kidney are likely non-hypoxic in CKD, as we observed with pimonidazole staining. To ensure that the global downregulation of the HIF pathway was not model-specific, we repeated the protein expression analysis in the classical unilateral urinary tract obstruction model (UUO) and observed similar results (**Supplementary Figure 3**). Finally, in a recent database of single-nuclei RNA sequencing in biopsies from CKD patients, we observed a global decreased of the hypoxia PROGENy pathway in proximal tubular cells (**Figure 2G and Supplementary Figure 4**), confirming that HIF pathway is not activated but rather downregulated during CKD.

The asparaginyl hydroxylase FIH is upregulated during CKD

In order to understand the downregulation of HIF targets genes despite some areas of hypoxia, we further assessed the expression of HIF hydroxylases. We observed that FIH was upregulated according to CKD severity in the Kröner-Fresenius databank of 217 CKD biopsies, while prolyl hydroxylases were either not regulated or downregulated (**Figure 3A**). In the same cohort, we observed a global decrease in HIF- α targets genes, EPO, PGK1 and GLUT1. HIF-1 α mRNA was upregulated, probably as a compensatory mechanism (43). We confirmed the upregulation of FIH protein expression in 15 consecutive random CKD biopsies from the Geneva University Hospitals clinical pathology department (**Figure 3B**). Automated quantification of FIH expression was correlated with kidney function loss (**Figure 3C and Supplementary Figure 5A-C**) and the staining was strong in proximal tubular cells during CKD (**Supplementary Figure 5 D**). In our murine models, FIH was also upregulated at the protein level (**Figure 3D-G**).

FIH is an important metabolic regulator *in vitro*

As FIH is upregulated according to CKD severity, we hypothesized that FIH could play a direct pathogenic role in CKD progression. FIH is a known metabolic regulator (19), which we confirmed in mouse derived kidney tubular cells (mpkccd) cell line. We found that FIH overexpression (**Figure 4A**) influenced the regulation of PGC1 α and CPT2, genes involved in mitochondrial biogenesis, mitochondrial function and lipid metabolism (**Figure 4B**). It also affects the mitochondrial reserve

capacity of mpkCCD cells (**Figure 4C**), as previously described in other cell types (44). We found opposite results with FIH silencing using siRNA in the same kidney cell line (**Figure 4D-E**), confirming that FIH affects cellular metabolism also in renal cells. Finally, we isolated cortical cells from 72 hours DM-NOFD treated mice and found an increased oxygen consumption rate globally (**Figure 4F**), confirming an important metabolic role of FIH in the kidney.

Pharmacologic inhibition of FIH in proteinuric CKD

The dimethyl ester of N-oxalyl-D-phenylalanine (DM-NOFD) is a small molecule inhibitor targeting preferentially FIH (45)(46). Its inhibitory effect on FIH is well-described *in vitro*, but has to our knowledge not been tested in animals before as a whole-body application. We found that a regimen of 200mg/kg each 24h during 28 days inhibited efficiently a downstream target of the Notch pathway, Hey1 (**Figure 5A**), without affecting EPO levels (**Supplementary Figure 6A**). In our model of proteinuric CKD, DM-NOFD globally increases the glomerular filtration rate of mice in the POD-ATTAC and control group (**Figure 5B**). This increase in glomerular filtration rate is not accompanied by an increased albuminuria (**Supplementary Figure 6B**). We also observe an alleviation of fibrosis development, as assessed by Sirius Red staining and quantification (**Figure 5C**) and western blotting of fibronectin and α SMA (**Figure 5D**). Although an important variability is present, preventing a statistical significance, we observe a global tendency to alleviate pro-inflammatory and pro-fibrotic markers by qPCR as well (**Figure 5E and Supplementary Figure 6C**).

DISCUSSION

Hypoxia has been described as a major mechanism causing the progression of CKD (5,47). This hypothesis has been raised according to the observation of decreased vascularization in progressive renal disease. However, this hypothesis does not consider the important role of tubular cells as energy consumers in the kidney. Indeed, the metabolic state of cells largely influence local oxygen consumption and therefore HIF pathway activation. Decreased vascularization, although present, may not lead to oxygen deficiency in all kidney areas given the fact that energy demand decreases in parallel in areas of tubular atrophy. Using a model of progressive proteinuric CKD, we show that hypoxia is not present in early stages of CKD; at late stages, hypoxia is preferentially localized in

remnant nephrons rather than in fibrotic zones. High-definition three-dimensional imaging of kidney microvasculature revealed a loss of capillaries mainly in the inner stripe of the outer medulla, however 98% of the analyzed kidney tissue was close enough (100 μ m) from a vessel to be within the oxygen diffusion limit of healthy tissue. We note that stating this limit presumes unchanged diffusion characteristics between healthy and diseased tissue. While it is conceivable that the limit may be altered in disease, we are not aware of reliable in vivo data on oxygen diffusion coefficients for fibrotic renal tissue

Besides hypoxia, the role of the HIF pathway in CKD has been debated and interventional studies in CKD models yielded mixed results. Genetic modulations of HIF expression indicate a detrimental role whereas pharmacological modulations show overall a protective effect (7). In diabetic nephropathy, an insufficient HIF-1 α activation was proposed as a factor of progression (48) and the efficiency of HIF-PHIs in renal anemia treatment also points towards a suboptimal activation (13). In our models, we show that HIF-1 α protein levels and its pathway are generally decreased, at early and late stages of CKD, despite a paradoxical downregulation of classical PHDs expression. This was observed in two animal models as well as in two dataset issued from biopsies of CKD patients. The cause of this downregulation is unclear and does not seem dependent on classical PHDs, which were themselves downregulated. FIH is a key regulator of HIF transcription, known to be expressed at baseline in the distal nephron where it may avoid continuous activation of the HIF pathway (50). In murine models and in human CKD, FIH was largely overexpressed in early and advanced CKD (16), especially in the proximal tubules and interstitial cells. Although other regulators of HIF may still participate in the observed HIF inhibition, the overexpression of FIH is expected to play an important role in HIF pathway inhibition, as well as on metabolism and inflammation regulation..

FIH has been described as a key regulator of metabolism, affecting especially lipid and mitochondrial metabolism, via modulations of the AMPK and PGC1 α pathways among others (19,29)(51). In cells, the modulation of FIH expression affected genes involved in fatty acid oxidation and mitochondrial biogenesis, such as PGC1 α , and influenced functionally the mitochondrial respiration. Mitochondrial dysfunction and downregulation of fatty acid oxidation are major factors leading to CKD progression, as reviewed elsewhere (52). A direct pathogenic role of FIH in CKD progression is therefore possible.

As HIF pathway modulation had a differential effect on CKD progression depending on the approach used, with a more favorable effect expected with pharmacologic modulations, we tested *in vivo* a specific FIH inhibitor, the DM-NOFD. To our knowledge, this specific compound has not been tested *in vivo* before. In mice, 200mg/kg of DM-NOFD each 24 hours intraperitoneally efficiently inhibited FIH protein expression and increased the glomerular filtration rate at baseline, an effect similar to the protective knock-in of PGC1 α , that could be mediated by the metabolic properties of FIH which we show *in vitro* and *in vivo* by seahorse analysis (53). The exact cause of the enhancement of GFR at baseline is however unclear and no albuminuria was observed. In our model of proteinuric CKD, DM-NOFD also tended to improve the loss of renal function, in terms of glomerular filtration rate and fibrosis development. Altogether, our results indicate that DM-NOFD efficiently inhibits FIH *in vivo*, is well-tolerated and could be protective in a model of proteinuric CKD. Studies with more animals and morphological histology data will be further performed to confirm our hypothesis.

In summary, we show that hypoxia is not an early phenomenon in CKD, and is mainly located in remnant nephrons. The HIF pathway is generally downregulated during CKD, and increased FIH expression may participate to this regulation. Finally, inhibiting FIH preferentially may play a protective role in CKD progression.

ACKNOWLEDGEMENTS

Else Kröner-Fresenius Foundation supported the European Renal cDNA Bank - Kröner-Fresenius biopsy bank (ERCB-KFB), for which we thank as well as all participating centers and their patients for their cooperation.

We are grateful to Marta Girona Alarcón for assisting with micro-CT imaging and the MiNa Core Facility for providing the equipment, Álvaro Gomariz Carrillo for consulting on the statistical image analysis, Diego Rossinelli for developing the image processing software and Tor Hildebrand for technical support.

We thank Phillip E. Sherer (Texas A&M Health Science Center School of Medicine Bryan/College Station, Texas) who kindly provided us with the POD-ATTAC mouse model.

We are also grateful to Thomas Cagarelli from the department of Pathology and the Genomics Platform at University of Geneva, Switzerland, Dr. Christelle Veyrat-Durebex from the Mouse Phenotyping Platform of the University of Geneva, Switzerland, and the whole Bioimaging Core Facility team of the University of Geneva, Switzerland.

CONFLICT OF INTEREST STATEMENT

Anna Faivre and Sophie de Seigneux received consulting fees from Astellas AG, Switzerland. Sophie de Seigneux received consulting fees from Bayer, Astra Zeneca, Otsuka. The other authors have no conflicts of interest to declare. The authors confirm that the results presented in this paper have not been published previously in whole or part, except in abstract format.

DATA AVAILABILITY STATEMENT

The data underlying this article will be shared on reasonable request to the corresponding author.

AUTHORS' CONTRIBUTIONS

A.F. and R.D. performed experiments, analyzed and interpreted data, drafted and revised the manuscript. W.K. designed and performed the micro-CT experiment, analyzed and interpreted data. T.V. and D.L. analyzed and interpreted data, and provided intellectual input. G.A. performed experiments and analyzed data. C.H. and M.F. performed experiments. R.D.R. analyzed and interpreted data. V.D. performed experiments and provided data. N.A.L. and B.S. provided the XlinCA contrast agent. G.S. and B.M. designed the micro-CT experiment. M.L. and C.C. generated and analyzed the microarray data from Kröner-Fresenius databank. J.M.R. provided with the POD-ATTAC mice. S.M. analyzed and interpreted data. C.C.S. and V.K. participated in the conception and design of the study and provided with reagents, analytical tools and intellectual input. S.D.S. designed and supervised the project. All authors revised the manuscript and approved of the final version to be published.

FUNDING

This study was supported by the NCCR.kidney.CH. SdS is supported by grants from the Swiss National Science Foundation (SNSF PP00P3-187186/1 and 320030_204187), Jules Thorn Foundation and NCCR Kidney.CH. AF is the recipient of a grant from the Swiss National Science Foundation (SNSF 323530_191224) and from the Carlos and Elsie de Reuter Foundation. DL and SdS are supported by a HUG *STARTER grant* no. RS03-25. WK was supported by the Swiss National Science Foundation (SNSF 205321_153523). DL received a Young Researcher Grant from Geneva University Hospitals (PRD 5-2020-I) and a grant from the Ernst and Lucie Schmidheiny foundation. The ERCB-KFB was supported by the Else Kröner-Fresenius Foundation. We also thank all participating centres of the European Renal cDNA Bank - Kröner-Fresenius biopsy bank (ERCB-KFB) and their patients for their cooperation.

ORIGINAL UNEDITED MANUSCRIPT

REFERENCES

1. Levey AS, Coresh J, Greene T, Stevens LA, Zhang Y (Lucy), Hendriksen S, et al. Using Standardized Serum Creatinine Values in the Modification of Diet in Renal Disease Study Equation for Estimating Glomerular Filtration Rate. *Ann Intern Med.* 2006 Aug 15;145(4):247.
2. Chen TK, Knicely DH, Grams ME. Chronic Kidney Disease Diagnosis and Management: A Review. *JAMA.* 2019 Oct 1;322(13):1294–304.
3. Kitiyakara C, Kopp JB, Eggers P. Trends in the epidemiology of focal segmental glomerulosclerosis. *Semin Nephrol.* 2003 Mar;23(2):172–82.
4. Hallan SI, Ritz E, Lydersen S, Romundstad S, Kvenild K, Orth SR. Combining GFR and albuminuria to classify CKD improves prediction of ESRD. *J Am Soc Nephrol JASN.* 2009 May;20(5):1069–77.
5. Fine LG, Norman JT. Chronic hypoxia as a mechanism of progression of chronic kidney diseases: from hypothesis to novel therapeutics. *Kidney Int.* 2008 Oct;74(7):867–72.
6. Palazon A, Goldrath A, Nizet V, Johnson RS. HIF Transcription Factors, Inflammation, and Immunity. *Immunity.* 2014 Oct 16;41(4):518–28.
7. Faivre A, Scholz CC, de Seigneux S. Hypoxia in chronic kidney disease: towards a paradigm shift? *Nephrol Dial Transplant* 2021 Oct;36(10):1782–90
8. Doi K, Noiri E, Fujita T. Role of vascular endothelial growth factor in kidney disease. *Curr Vasc Pharmacol.* 2010 Jan;8(1):122–8.
9. Nordquist L, Friederich-Persson M, Fasching A, Liss P, Shoji K, Nangaku M, et al. Activation of hypoxia-inducible factors prevents diabetic nephropathy. *J Am Soc Nephrol JASN.* 2015 Feb;26(2):328–38.
10. Nayak BK, Shanmugasundaram K, Friedrichs WE, Cavaglieri RC, Patel M, Barnes J, et al. HIF-1 Mediates Renal Fibrosis in OVE26 Type 1 Diabetic Mice. *Diabetes.* 2016 May;65(5):1387–97.
11. Katavetin P, Miyata T, Inagi R, Tanaka T, Sassa R, Ingelfinger JR, et al. High Glucose Blunts Vascular Endothelial Growth Factor Response to Hypoxia *via* the Oxidative Stress-Regulated Hypoxia-Inducible Factor/Hypoxia-Responsible Element Pathway. *J Am Soc Nephrol.* 2006 May;17(5):1405–13.
12. Chen N, Hao C, Peng X, Lin H, Yin A, Hao L, et al. Roxadustat for Anemia in Patients with Kidney Disease Not Receiving Dialysis. *N Engl J Med.* 2019 12;381(11):1001–10.
13. Chen N, Hao C, Liu BC, Lin H, Wang C, Xing C, et al. Roxadustat Treatment for Anemia in Patients Undergoing Long-Term Dialysis. *N Engl J Med.* 2019 Sep 12;381(11):1011–22.
14. Shutov E, Sułowicz W, Esposito C, Tataradze A, Andric B, Reusch M, et al. Roxadustat for the treatment of anemia in chronic kidney disease patients not on dialysis: a phase 3, randomized, double-blind, placebo-controlled study (ALPS). *Nephrol Dial Transplant* 2021 Sept;36(9):1629–39
15. Lando D, Peet DJ, Gorman JJ, Whelan DA, Whitelaw ML, Bruick RK. FIH-1 is an asparaginyl hydroxylase enzyme that regulates the transcriptional activity of hypoxia-inducible factor.

Genes Dev. 2002 Jun 15;16(12):1466–71.

16. Mahon PC, Hirota K, Semenza GL. FIH-1: a novel protein that interacts with HIF-1 α and VHL to mediate repression of HIF-1 transcriptional activity. *Genes Dev.* 2001 Oct 15;15(20):2675–86.
17. Hewitson KS, McNeill LA, Riordan MV, Tian YM, Bullock AN, Welford RW, et al. Hypoxia-inducible factor (HIF) asparagine hydroxylase is identical to factor inhibiting HIF (FIH) and is related to the cupin structural family. *J Biol Chem.* 2002 Jul 19;277(29):26351–5.
18. Sim J, Cowburn AS, Palazon A, Madhu B, Tyrakis PA, Macías D, et al. The Factor Inhibiting HIF Asparaginyl Hydroxylase Regulates Oxidative Metabolism and Accelerates Metabolic Adaptation to Hypoxia. *Cell Metab.* 2018 Apr;27(4):898-913.e7.
19. Zhang N, Fu Z, Linke S, Chicher J, Gorman JJ, Visk D, et al. The Asparaginyl Hydroxylase Factor Inhibiting HIF-1 α Is an Essential Regulator of Metabolism. *Cell Metab.* 2010 May;11(5):364–78.
20. Yu X, Fang Y, Ding X, Liu H, Zhu J, Zou J, et al. Transient hypoxia-inducible factor activation in rat renal ablation and reduced fibrosis with L-mimosine. *Nephrol Carlton Vic.* 2012 Jan;17(1):58–67.
21. Yu X, Fang Y, Liu H, Zhu J, Zou J, Xu X, et al. The balance of beneficial and deleterious effects of hypoxia-inducible factor activation by prolyl hydroxylase inhibitor in rat remnant kidney depends on the timing of administration. *Nephrol Dial Transplant.* 2012 Aug;27(8):3110–9.
22. Rutkowski JM, Wang ZV, Park ASD, Zhang J, Zhang D, Hu MC, et al. Adiponectin Promotes Functional Recovery after Podocyte Ablation. *J Am Soc Nephrol.* 2013 Feb 1;24(2):268–82.
23. Rajaram RD, Dissard R, Faivre A, Ino F, Delitsikou V, Jaquet V, et al. Tubular NOX4 expression decreases in chronic kidney disease but does not modify fibrosis evolution. *Redox Biol.* 2019;26:101234.
24. Faivre A, Katsyuba E, Verissimo T, Lindenmeyer M, Rajaram RD, Naesens M, et al. Differential role of nicotinamide adenine dinucleotide deficiency in acute and chronic kidney disease. *Nephrol Dial Transplant* 2021 Jan;36(1):60–8
25. Schreiber A, Shulhevich Y, Geraci S, Hesser J, Stsepankou D, Neudecker S, et al. Transcutaneous measurement of renal function in conscious mice. *Am J Physiol-Ren Physiol.* 2012 Sep;303(5):F783–8.
26. Fila M, Brideau G, Morla L, Cheval L, Deschênes G, Doucet A. Inhibition of K⁺ secretion in the distal nephron in nephrotic syndrome: possible role of albuminuria. *J Physiol.* 2011 Jul 15;589(Pt 14):3611–21.
27. Dizin E, Hasler U, Nlandu-Khodo S, Fila M, Roth I, Hernandez T, et al. Albuminuria induces a proinflammatory and profibrotic response in cortical collecting ducts via the 24p3 receptor. *Am J Physiol Renal Physiol.* 2013 Oct 1;305(7):F1053-1063.
28. Delitsikou V, Jarad G, Rajaram RD, Ino F, Rutkowski JM, Chen CD, et al. Klotho regulation by albuminuria is dependent on ATF3 and endoplasmic reticulum stress. *FASEB J.* 2020;34(2):2087–104.

29. Scholz CC, Rodriguez J, Pickel C, Burr S, Fabrizio J alba, Nolan KA, et al. FIH Regulates Cellular Metabolism through Hydroxylation of the Deubiquitinase OTUB1. Simon C, editor. *PLOS Biol.* 2016 Jan 11;14(1):e1002347.
30. Pickel C, Günter J, Ruiz-Serrano A, Spielmann P, Fabrizio JA, Wolski W, et al. Oxygen-dependent bond formation with FIH regulates the activity of the client protein OTUB1. *Redox Biol.* 2019;26:101265.
31. Verissimo T, Faivre A, Rinaldi A, Lindenmeyer M, Delitsikou V, Veyrat-Durebex C, et al. Decreased Renal Gluconeogenesis Is a Hallmark of Chronic Kidney Disease. *J Am Soc Nephrol JASN.* 2022 Apr;33(4):810–27.
32. Cohen CD, Klingenhoff A, Boucherot A, Nitsche A, Henger A, Brunner B, et al. Comparative promoter analysis allows *de novo* identification of specialized cell junction-associated proteins. *Proc Natl Acad Sci.* 2006 Apr 11;103(15):5682–7.
33. Shved N, Warsow G, Eichinger F, Hoogewijs D, Brandt S, Wild P, et al. Transcriptome-based network analysis reveals renal cell type-specific dysregulation of hypoxia-associated transcripts. *Sci Rep.* 2017 Dec;7(1):8576.
34. Tusher VG, Tibshirani R, Chu G. Significance analysis of microarrays applied to the ionizing radiation response. *Proc Natl Acad Sci U S A.* 2001 Apr 24;98(9):5116–21.
35. Kuo W, Le NA, Spingler B, Wenger RH, Kipar A, Hetzel U, et al. Simultaneous Three-Dimensional Vascular and Tubular Imaging of Whole Mouse Kidneys With X-ray μ CT. *Microsc Microanal.* 2020 Aug;26(4):731–40.
36. Le NA, Kuo W, Müller B, Kurtcuoglu V, Spingler B. Crosslinkable polymeric contrast agent for high-resolution X-ray imaging of the vascular system. *Chem Commun.* 2020 Jun 2;56(44):5885–8.
37. Chiefari J, Chong YK (Bill), Ercole F, Krstina J, Jeffery J, Le TPT, et al. Living Free-Radical Polymerization by Reversible Addition–Fragmentation Chain Transfer: The RAFT Process. *Macromolecules.* 1998 Aug 1;31(16):5559–62.
38. Lai JT, Filla D, Shea R. Functional Polymers from Novel Carboxyl-Terminated Trithiocarbonates as Highly Efficient RAFT Agents. *Macromolecules.* 2002 Aug 1;35(18):6754–6.
39. Schindelin J, Arganda-Carreras I, Frise E, Kaynig V, Longair M, Pietzsch T, et al. Fiji: an open-source platform for biological-image analysis. *Nat Methods.* 2012 Jul;9(7):676–82.
40. Schneider CA, Rasband WS, Eliceiri KW. NIH Image to ImageJ: 25 years of image analysis. *Nat Methods.* 2012 Jul;9(7):671–5.
41. Schubert M, Klfinger B, Klünemann M, Sieber A, Uhlitz F, Sauer S, et al. Perturbation-response genes reveal signaling footprints in cancer gene expression. *Nat Commun.* 2018 Dec;9(1):20.
42. Kuo W, Le NA, Spingler B, Wenger RH, Kipar A, Hetzel U, et al. Simultaneous Three-Dimensional Vascular and Tubular Imaging of Whole Mouse Kidneys With X-ray μ CT. *Microsc Microanal Off J Microsc Soc Am Microbeam Anal Soc Microsc Soc Can.* 2020 Aug;26(4):731–40.
43. Wenger RH, Kvietikova I, Rolfs A, Gassmann M, Marti HH. Hypoxia-inducible factor-1 alpha is regulated at the post-mRNA level. *Kidney Int.* 1997 Feb;51(2):560–3.

44. Sim J. et al. The Factor Inhibiting HIF Asparaginyl Hydroxylase. *Cell Metabolism*. 2018 Apr;27(4):898–913.
45. McDonough MA, McNeill LA, Tilliet M, Papamicaël CA, Chen QY, Banerji B, et al. Selective inhibition of factor inhibiting hypoxia-inducible factor. *J Am Chem Soc*. 2005 Jun 1;127(21):7680–1.
46. Sulser P, Pickel C, Günter J, Leissing TM, Crean D, Schofield CJ, et al. HIF hydroxylase inhibitors decrease cellular oxygen consumption depending on their selectivity. *FASEB J* 2020 Feb; 34(2):2344–58.
47. Eddy AA. Overview of the cellular and molecular basis of kidney fibrosis. *Kidney Int Suppl*. 2014 Nov;4(1):2–8.
48. Catrina SB, Zheng X. Hypoxia and hypoxia-inducible factors in diabetes and its complications. *Diabetologia*. 2021 Apr 1;64(4):709–16.
49. Yamaguchi J, Tanaka T, Eto N, Nangaku M. Inflammation and hypoxia linked to renal injury by CCAAT/enhancer-binding protein δ . *Kidney Int*. 2015 Aug;88(2):262–75.
50. Schödel J, Bohr D, Klanke B, Schley G, Schlötzer-Schrehardt U, Warnecke C, et al. Factor inhibiting HIF limits the expression of hypoxia-inducible genes in podocytes and distal tubular cells. *Kidney Int*. 2010 Nov;78(9):857–67.
51. Ruiz-Serrano A, Boyle C, Monné Rodríguez J, Günter J, Jucht A, Pfundstein S, et al. The Deubiquitinase OTUB1 Is a Key Regulator of Energy Metabolism. *Int J Mol Sci*. 2022 Jan 28;23(3):1536.
52. Jang HS, Noh MR, Kim J, Padanilam BJ. Defective Mitochondrial Fatty Acid Oxidation and Lipotoxicity in Kidney Diseases. *Front Med* 2020 Mar 12; 7:65
53. Han SH, Wu MY, Nam BY, Park JT, Yoo TH, Kang SW, et al. PGC-1 α Protects from Notch-Induced Kidney Fibrosis Development. *J Am Soc Nephrol JASN*. 2017 Nov;28(11):3312–22.

Figure 1.

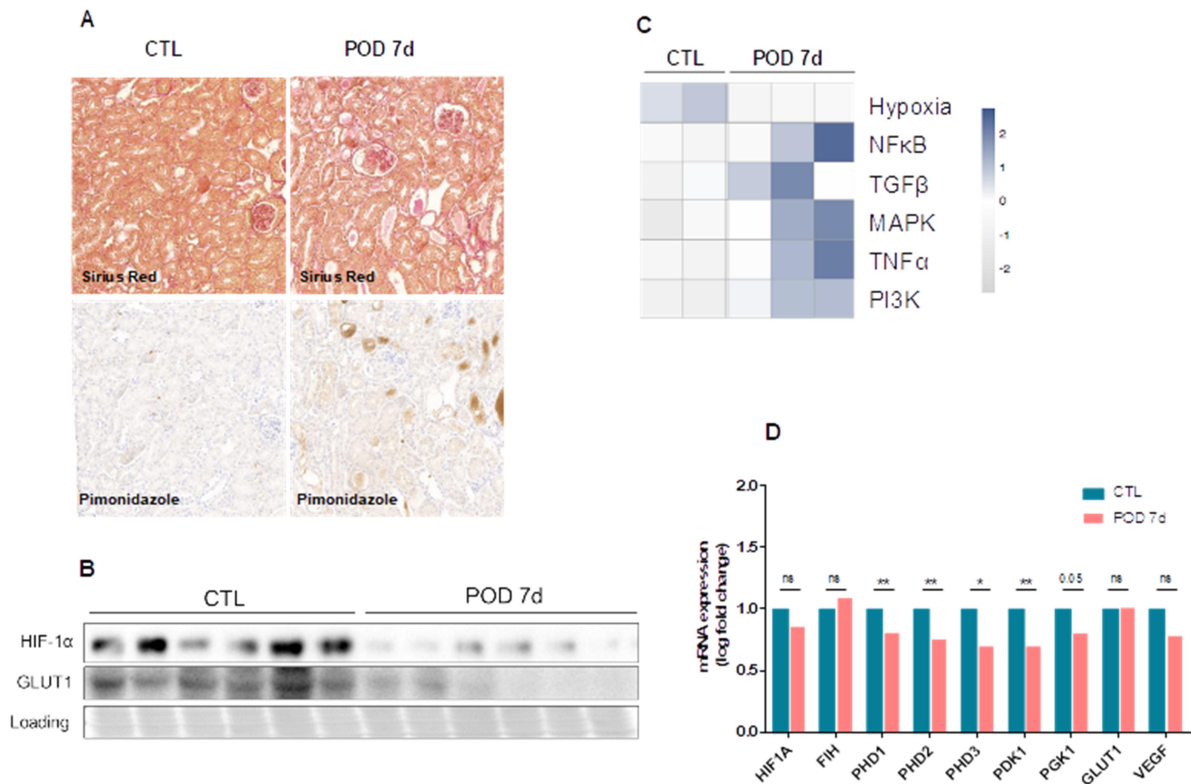


Figure 1. Early stages of proteinuric CKD are not characterized by hypoxia and HIF activation

(A) Representative serial sections of control (CTL) and POD-ATTAC mice 7 days after a single-dose of dimerizer injection (POD 7d). In the upper panel, Sirius Red staining and in the lower panel, pimonidazole immunohistochemistry are shown.

(B) Representative immunoblot of kidney cortex in CTL (n=6) and POD 7d (n=6) mice for HIF-1α and GLUT1.

(C) RNA sequencing analysis in CTL (n=2) and POD 7d mice (n=3) and corresponding heatmap of Progeny pathways (Hypoxia, NFκB, TGFβ, MAPK, TNFα, PI3K).

(D) mRNA expression assessed by qPCR in CTL (n=6) and POD 7d (n=6) of HIF-1 α , FIH, PHD1, PHD2, PHD3, PDK1, PGK1, GLUT1, VEGF.

Results are presented as fold change compared to controls, with error-bars showing mean \pm standard deviation. * p<0.05, ** p<0.01

ORIGINAL UNEDITED MANUSCRIPT

Figure 2.

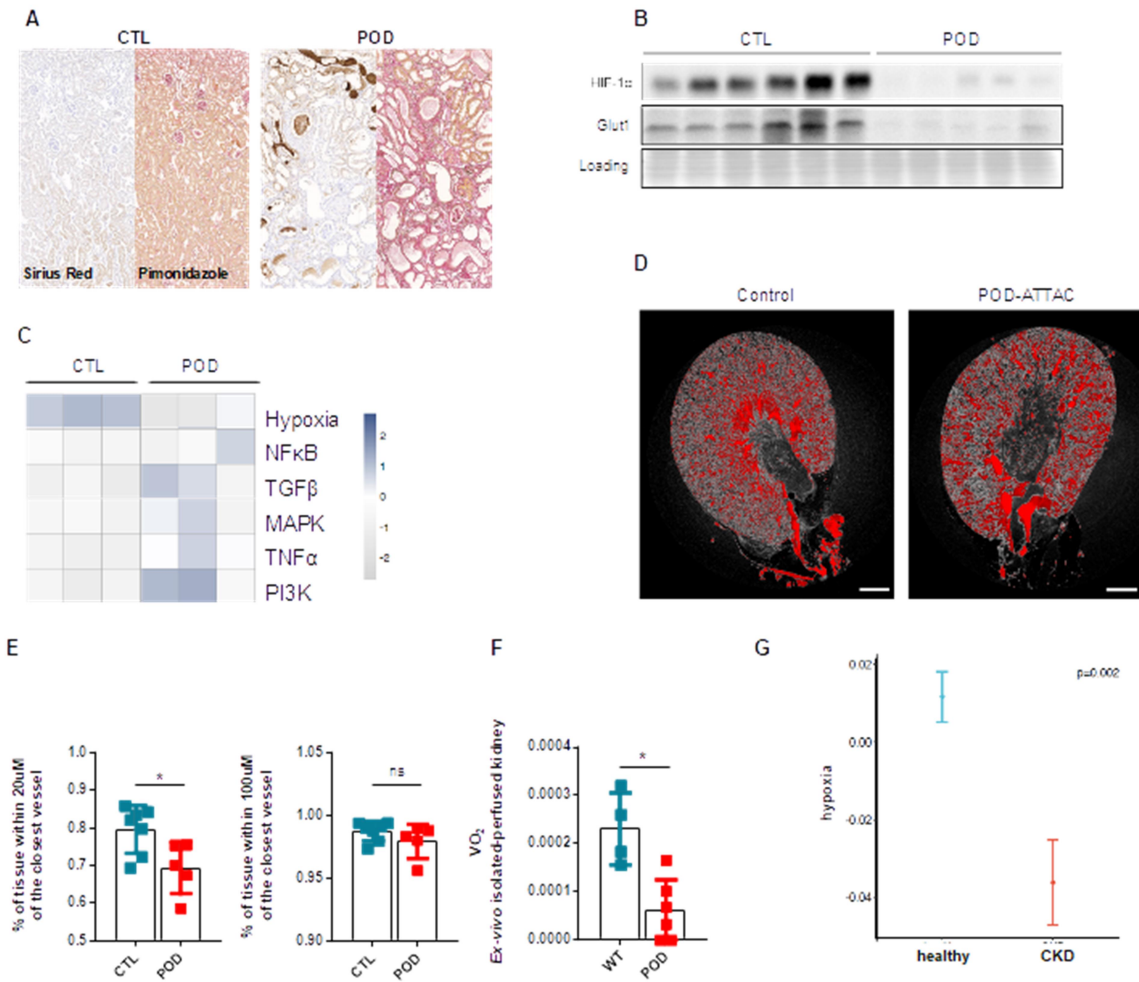


Figure 2. In late stages of proteinuric CKD, vascularization is rarefied but does not induce a major hypoxia

(A) Representative serial sections of control (CTL) and POD-ATTAC mice 28 days after repeated injections of dimerizer (POD). In the left panel, Sirius Red staining and in the right panel, pimonidazole immunohistochemistry.

(B) Representative immunoblot of kidney cortex in CTL (n=6) and POD (n=5) mice for HIF-1α and GLUT1 and corresponding loading control (Ponceau S staining).

(C) RNA sequencing analysis in CTL (n=3) and POD mice (n=3) and corresponding heatmap of Progeny pathways (Hypoxia, NFkB, TGFβ, MAPK, TNFa, PI3K).

(D) Representative visualization of renal microvascularization assessed by micro-CT imaging following contrast agent perfusion.

(E) Percentage of kidney tissue within 20μm or 100μm of the closest blood vessel, quantified by micro-CT following contrast agent perfusion, in CTL (n=7) and POD (n=5) kidneys. *p<0.05

(F) In the *ex-vivo* perfused kidney set-up, renal oxygen consumption (VO₂) in CTL (n=4) and POD (n=6) kidneys. *p<0.05

(G) Hypoxia PROGENy pathway in human FACS sorted PDGFRb+ analyzed by scRNA-seq indicating a global deactivation of the pathway in CKD (p=0.002)

Results are presented with error-bars showing mean ± standard deviation.

ORIGINAL UNEDITED MANUSCRIPT

Figure 3.

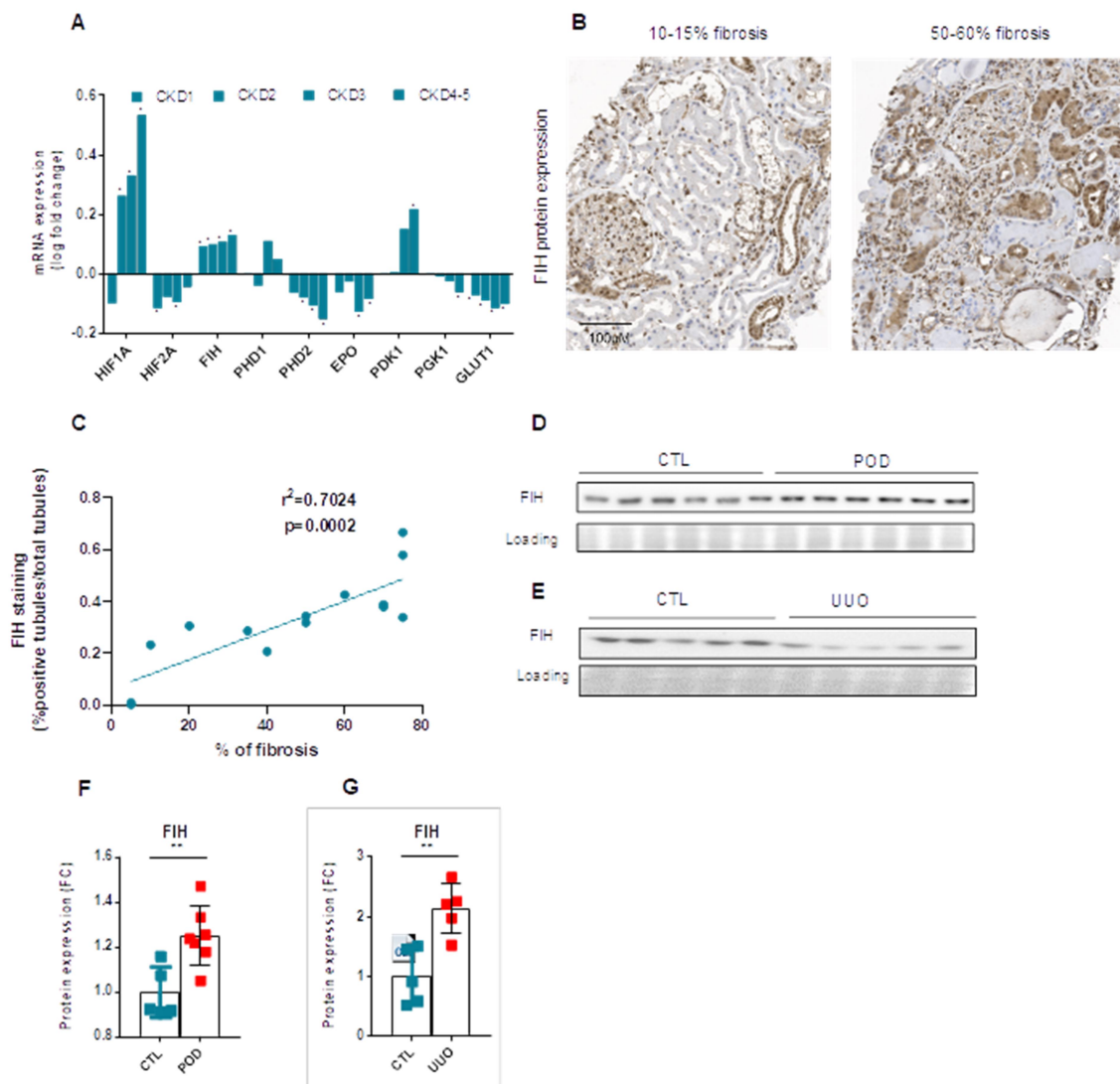


Figure 3. The asparaginyl hydroxylase FIH is upregulated during CKD

(A) Analysis of *HIF1A*, *HIF2A*, *FIH*, *PHD1*, *PHD2*, *PHD3*, *EPO*, *PDK1*, *PGK1*, *GLUT1* in the Affymetrix microarray expression dataset obtained in the European Renal cDNA Kröner-Fresenius Biopsy bank, sorted by chronic kidney disease (CKD) stage (CKD1, n = 56; CKD2, n = 46; CKD3, n = 37; CKD4, n = 26; CKD5, n = 10). Biopsies from kidney donors (n=42) are used as controls. * $q < 0.05$.

(B) Representative immunostaining of FIH in human kidney biopsies according to fibrosis level assessed by an experienced renal pathologist (left panel: 10-15% of fibrosis; right panel: 50-60% of fibrosis).

(C) Automated quantification of FIH staining with QuPath and relative correlation with estimated glomerular filtration rate by creatinine CKD-EPI (eGFR) equation, in kidney biopsies from 15 CKD patients (fibrosis less than 20%, n=5; between 40% to 50%, n=5 and more than 70%, n=4), fitted through linear regression ($r^2=0.7024$)

(D) Representative immunoblot of kidney cortex in CTL (n=6) and POD (n=5) mice for FIH and corresponding loading control (Ponceau S staining).

(E) Representative immunoblot of kidney cortex in contralateral kidneys (CTL, n=6) and in kidneys after 5 days of unilateral urethral obstruction (UUO, n=5) for FIH and corresponding loading control (Ponceau S staining).

(F) Protein expression quantification of kidney cortex in CTL (n=6) and POD (n=5) mice for FIH and corresponding loading control (Ponceau S staining).

(G) Protein expression quantification of kidney cortex in contralateral kidneys (CTL, n=6) and in kidneys after 5 days of unilateral urethral obstruction (UUO, n=5) for FIH and corresponding loading control (Ponceau S staining). ** $p<0.01$

Results are presented with error-bars showing mean \pm standard deviation.

Figure 4.

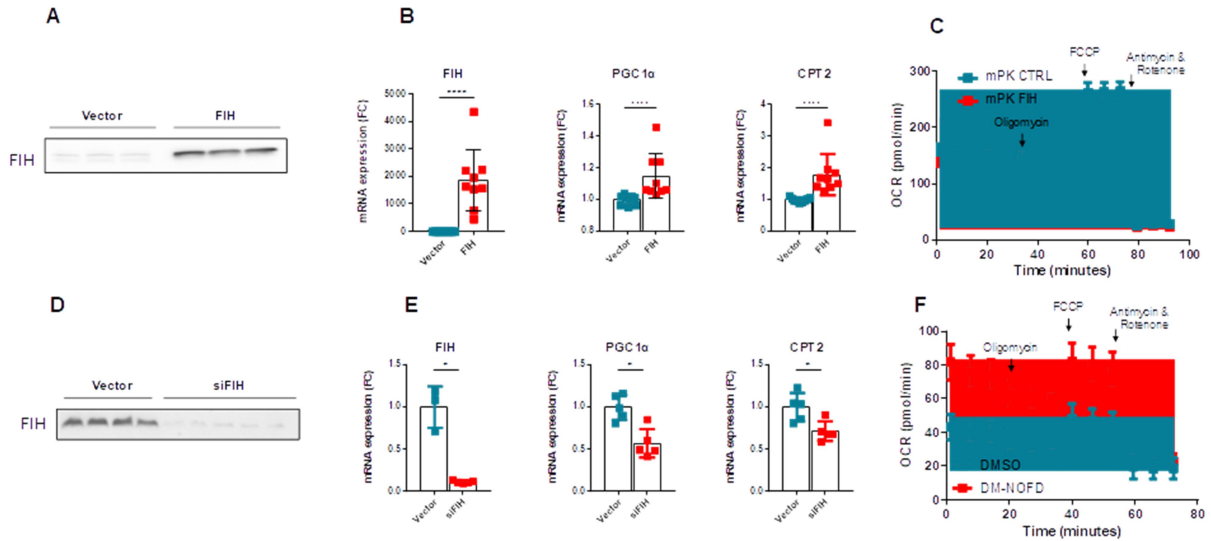


Figure 4. FIH is an important metabolic regulator *in vitro*

(A) Representative immunoblot of FIH in mCCD-cl1 cells transfected with control plasmid (vector, n=3) or plasmid encoding for human FIH (FIH, n=3).

(B) mRNA expression assessed by RT-qPCR of FIH, PGC1α and CPT2 in mCCD-cl1 cells transfected with control plasmid (vector, n=9) or plasmid encoding for human FIH (FIH, n=9). **** $p < 0.0001$.

(C) Oxidative stress test, showing the oxygen consumption rate of mPKCCD cells transfected with control plasmid (mPK CTRL) or plasmid encoding for human FIH (mPK FIH) and subjected to oligomycin, carbonyl cyanide-p-trifluoromethoxyphenylhydrazone (FCCP) and antimycin/rotenone.

(D) Representative immunoblot of FIH in HK-2 cells transfected with control siRNA (vector, n=4) or siRNA targeting FIH (siFIH, n=4).

(E) mRNA expression assessed by RT-qPCR of FIH, PGC1α and CPT2 in HK-2 cells transfected with control siRNA (vector, n=5) or siRNA targeting FIH (siFIH, n=5). * $p < 0.05$

(F) Oxidative stress test, showing the oxygen consumption rate of primary cultured tubular cells injected 72h prior experiment with DM-NOFD (DM-NOFD) or vehicle (DMSO) and subjected to oligomycin, carbonyl cyanide-p-trifluoromethoxyphenylhydrazone (FCCP) and antimycin/rotenone.

Results are presented with error-bars showing mean \pm standard deviation.

ORIGINAL UNEDITED MANUSCRIPT

Figure 5.

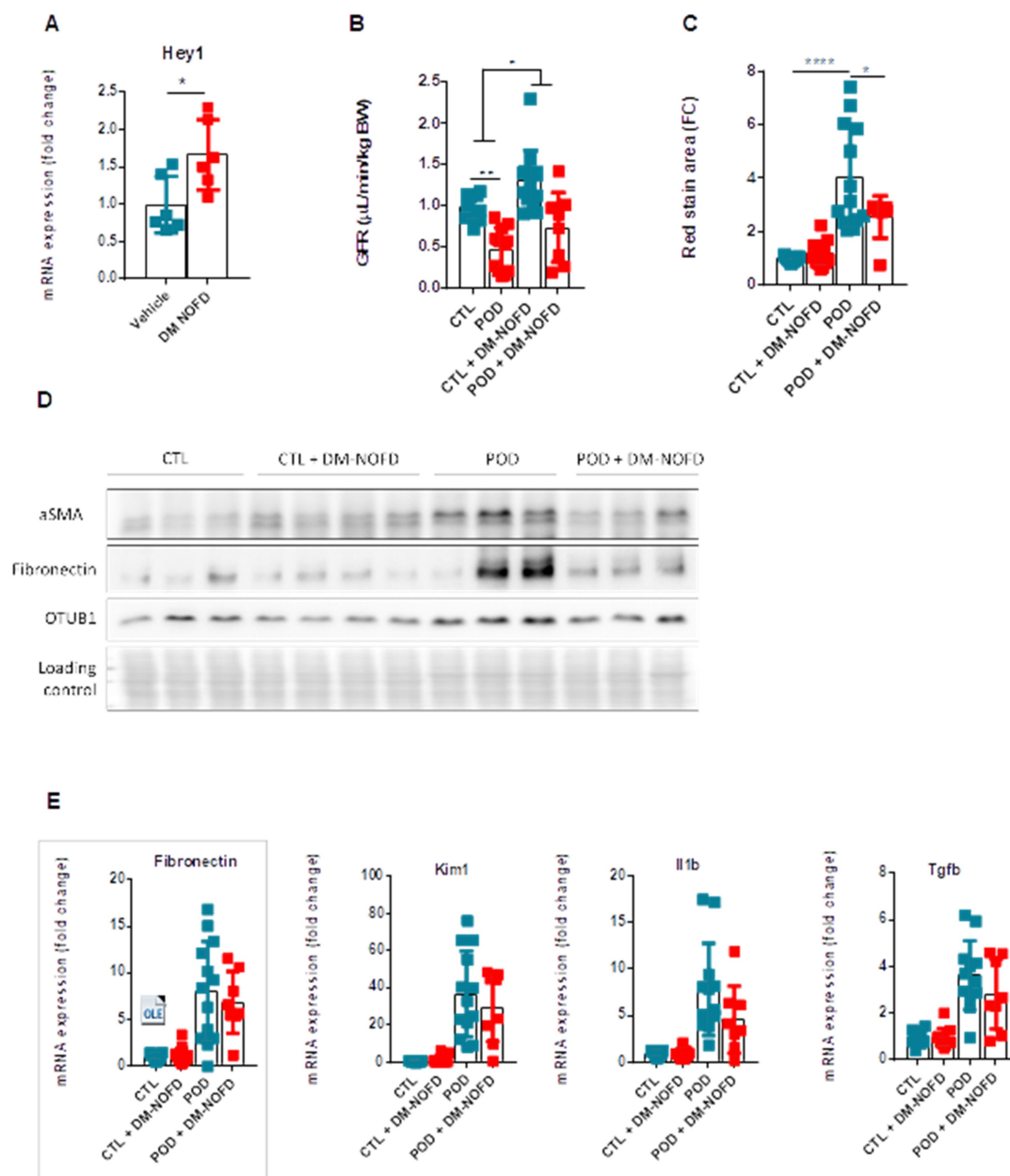


Figure 5. Pharmacologic inhibition of FIH in proteinuric CKD

(A) mRNA expression assessed by RT-qPCR of Hey1 in kidney cortex of mice treated with intraperitoneal injections of vehicle (DMSO 0.002%, n=6) or with 200mg/kg of DM NOFD. *p<0.05

(B) Glomerular filtration rate (GFR) assessed by sinistrin clearance in control mice treated with vehicle (CTL, n=9), POD-ATTAC mice 28 days after repeated dimerizer injections and treated with vehicle

ORIGINAL

(POD, n=12), control mice treated with 200mg/kg of DM-NOFD (CTL + DM-NOFD, n=13), and POD-ATTAC mice 28 days after repeated dimerizer injections and treated with 200mg/kg of DM-NOFD (POD + DM-NOFD, n=8). *p<0.05

(C) Quantification of Sirius red staining in CTL (n=9), POD (n=12), CTL + DM-NOFD (n=13), and POD + DM-NOFD (n=8). *p<0.05, ****p<0.0001.

(D) Representative immunoblot of kidney cortex in CTL (n=9), POD (n=12), CTL + DM-NOFD (n=13), and POD + DM-NOFD (n=8) for α SMA, Fibronectin and OTUB1 with corresponding loading control (Ponceau S staining).

(E) mRNA expression assessed by RT-qPCR in CTL (n=9), POD (n=12), CTL + DM-NOFD (n=13), and POD + DM-NOFD (n=8) of Fibronectin, Kim1, Il1b, and Tgfb genes.

ORIGINAL UNEDITED MANUSCRIPT